Synopsis The effect of Li^+ and Ta^{5+} on the crystal structure and electrical properties of $(K_xNa_{1-x})NbO_3$ ceramics has been investigated. The results from Rietveld refinement show that the presence of Li^+ suppresses the formation of the orthorhombic-tetragonal phase transition to low temperatures. Phase coexistence over wide temperature range may help to explain why the piezoelectric properties in doped $(K_xNa_{1-x})NbO_3$ ceramics are higher than in the undoped samples.

Electrical and structural characterization of $(K_xNa_{1-x})NbO_3$ ceramics modified with Li and Ta

Henry E. Mgbemere [I], Manuel Hinterstein [II] and Gerold A Schneider [I,*]

I Institute of Advanced Ceramics, Hamburg University of Technology, Denickestraße 15, 21073 Hamburg, Germany
II Institut für Werkstoffwissenschaften, Technische Universität Dresden, Helmholtzstraße 7, 01069 Dresden, Germany

Abstract $(K_xNa_{1-x})NbO_3$ ceramics modified with Li^+ and Ta^{5+} have been produced using the mixed-oxide synthesis method. Synchrotron X-ray diffraction measurements were made on the samples from 12K to temperatures above their ferroelectric-paraelectric transition points with 10K measurement steps. Rietveld refinement using FULLPROF suite was used to refine the patterns. Depending on the composition and temperature, rhomhohedral phases, orthorhombic phases, tetragonal phases, cubic phases and two-phase mixtures were obtained. *R3c* (161), *Amm2* (38), *P4mm* (99), $Pm\bar{3}m$ (221) space groups and their combinations were used to refine the rhombohedral, orthorhombic, tetragonal, cubic and the mixed phases respectively. Li^+ addition suppressed the formation of the rhombohedral low temperature phase and increased the Curie temperature. This is attributed to size difference in ionic radii of the A-site elements which leads to increased atomic polarizability and increased interaction with the B-site element. Li^+ and Ta^{5+} co-doping led to a wide temperature range of phase coexistence between the orthorhombic and tetragonal phase. Electrical characterizations by dielectric and hysteresis measurements were used to compare with the results from the structural studies.

Keywords: $(K_xNa_{1-x})NbO_3$; ferroelectric ceramics; phase transition, synchrotron radiation

[*] Correspondence author (g.schneider@tu-harburg.de)

1.0 Introduction

Lead zirconate titanate (PZT)-based ceramics are the most frequently used piezoelectric ceramics in devices for sensing, electromechanical and actuation purposes. Environmental safety awareness and legislations against continuing the use of lead has made it necessary that lead-free piezoelectric ceramic alternatives are used to replace PZT-based ceramics. The potential lead-free alternatives include; $BaTiO_3$ based ceramics (Hippel, 1950), $(Bi_{0.5}Na_{0.5})TiO_3$ based ceramics (Takenaka *et al.*, 1997; Ichinose & Udagawa, 1995) and $(K_xNa_{1-x})NbO_3$ (KNN) based ceramics (Egerton & Dillion, 1959). KNN is a solid solution of ferroelectric $KNbO_3$ and antiferroelectric $NaNbO_3$. It undergoes a series of phase transitions just like in $BaTiO_3$ and the structure of this composition has been well investigated (Shirane *et al.*, 1954; Lufaso *et al.*, 2006; Egerton & Dillion, 1959). It has a relatively high Curie temperature T_c (~ 420 °C) and moderate piezoelectric properties (~80 pC/N) (Egerton & Dillion, 1959). When other elements are added to this composition in the form of dopants, its sinterability and piezoelectric properties are improved while the phase transition temperatures are lowered in most cases (Saito *et al.*, 2004; Noheda *et al.*, 2000; Hagh *et al.*, 2008).

The effect of doping KNN with Li^+ has been investigated by a lot of researchers. Guo et al (Guo *et al.*, 2004) studied Li^+ addition from 4 to 20 mol %, and reported an increase in the piezoelectric properties but also showed that above 8 mol %, an extra phase ($K_3Li_2Nb_5O_{15}$) begins to form. High temperature dielectric studies (Zhao *et al.*, 2007; Klein *et al.*, 2007; Du *et al.*, 2007) have been used to investigate the changes in phase transition temperature with Li^+ addition while thermal cycling (Hollenstein *et al.*, 2007) was used to study its effect on the properties of KNN. Raman spectroscopy, dielectric and piezoelectric measurements were used to construct a phase diagram for Li^+ doped KNN ceramics and the authors reported the occurrence of a rhombohedral phase at very low temperatures (Klein *et al.*, 2007). Rietveld refinement using a two-phase model with space groups *Amm2* and *P4mm* was used to refine the crystal structure of this composition up to 6 mol % Li^+ at room temperature (Lee *et al.*, 2007).

Ta^{5+} was reported to lower both the electromechanical quality factor and the phase transition temperatures when added to KNN (Mgbemere *et al.*, 2010). It also decreased the grain size of KNN ceramics due to the high temperatures required for the sintering (Zuo *et al.*, 2009). There are some reports in the literature about the doping of KNN with both Li^+ and Ta^{5+} (Saito *et al.*, 2004; Hollenstein *et al.*, 2005). In one of the reports on KNN modified with 7 mol % $LiTaO_3$, *P1m1* space group was used as a reference material for the refinement of the patterns and the temperature dependent lattice parameters were obtained. An extra phase, however, can be observed in the diffraction pattern used for the Rietveld refinement

(Skidmore *et al.*, 2009). The piezoelectric and electromechanical properties of the samples are reported to be increased while their phase transition temperatures decreased.

There is not much information in the literature with regard to structural studies of modified KNN ceramics at both cryogenic and elevated temperatures. Synchrotron diffraction is a very important tool for studying structures of crystalline substances. In this investigation, KNN modified with Li^+, Ta^{5+} and a combination of Li^+ and Ta^{5+} was synthesized and analyzed from 12K to temperatures above their respective T_c. Dielectric and hysteresis measurements were also carried out on the samples. The objective of this article is to determine in these ceramics the relative amount of phases present, their lattice parameters, and phase transition temperatures from cryogenic temperatures to temperatures above their ferroelectric-paraelectric transition temperatures and to compare these results with those obtained through electrical characterization.

2.0 Experimental details

2.1 Sample preparation

The intended compositions to be produced using the conventional synthesis method are $(K_{0.48}Na_{0.48}Li_{0.04})NbO_3$, $(K_{0.5}Na_{0.5})(Nb_{0.9}Ta_{0.1})O_3$, $(K_{0.48}Na_{0.48}Li_{0.04})(Nb_{0.9}Ta_{0.1})O_3$. K_2CO_3, Na_2CO_3, Li_2CO_3 (99%), Nb_2O_5 and Ta_2O_5 (99.9%) (Chempur Feinchemikalien und Forschungs GmbH, Karlsruhe, Germany) are the raw powders used for the synthesis. The powders were dried at 200 °C, mixed, attrition milled for 4 h and calcined in air at 750 °C for 4 h. The milling step was repeated to ensure that a homogenous powder was obtained and to reduce the particle size. They were pressed into pellets with a cold isostatic press at 300 MPa for 2 min. The pellets were sintered in air at temperatures ranging from 1070 °C to 1100 °C for 1 h with a heating and cooling rate of 2 °C/min and 10 °C/min respectively. The pellets were ground for both chemical analysis and synchrotron X-ray diffraction measurements. In order to reduce residual stresses, the samples were annealed at 750 °C for 30 min.

Optical emission spectroscopy/Inductive coupled plasma (OES-ICP (PE-Optima 7000 DV)) analysis technique was used to determine the quantitative amount of each element present and search for possible impurities which may have been introduced during processing. A mean value was obtained from four separate measurements and the OES-ICP values as well as the element amount in moles are shown in Table 1. Due to sublimation during the sintering process as a result of high volatility of some elements, small amounts of some elements were lost.

Na^+, Ta^{5+} and O^{2-} in most cases either remained same or slightly higher than the calculated amounts before the synthesis while Li^+ and K^+ were lower. Since the starting powders were

not 100 % pure, it is possible that some of the powders contained small amounts of these elements in excess. The final compositions were adjusted to reflect the changes in the amounts of elements present after the chemical analysis. Grinding balls made from zirconia were used during the milling process and the chemical analysis showed that small amounts were introduced into the samples. Finally, we concluded that our compositions are actually; $(K_{0.47}Na_{0.51}Li_{0.03})(Nb_{0.97})O_{3.01}$ abbreviated as KNN-L, $(K_{0.49}Na_{0.51})$ $(Nb_{0.88}Ta_{0.1})O_3$ as KNN-T, and $(K_{0.47}Na_{0.51}Li_{0.025})$ $(Nb_{0.88}Ta_{0.1})O_{3.02}$ as KNN-LT.

Table 1 OES-ICP analysis data as well as calculated molar amounts of the elements in our composition.

Element	Li	Na	K	Nb	Ta	O	Zr*
$(K_{0.48}Na_{0.48}Li_{0.04})NbO_3$							
OES-ICP values [g/kg]	1.27 (3)	68.9 (14)	108 (22)	526 (11)		281 (6)	0.40
Element amount [mol]	0.03136	0.51369	0.47346	0.97041		3.01034	<0.00075
$(K_{0.5}Na_{0.5})$ $(Nb_{0.90}Ta_{0.1})O_3$							
OES-ICP values [g/kg]		64.5 (13)	105 (2)	452 (9)	98.2 (20)	266 (5)	0.40
Element amount [mol]		0.50957	0.48777	0.88364	0.09857	3.01966	<0.00080
$(K_{0.48}Na_{0.48}Li_{0.04})$ $(Nb_{0.9}Ta_{0.1})O_3$							
OES-ICP values [g/kg]	0.96 (2)	64.6 (13)	101 (2)	451 (9)	101 (2)	267 (5)	0.40
Element amount [mol]	0.02502	0.5083	0.46736	0.87825	0.10098	3.01922	<0.00079

2.2 Synchrotron X-ray data collection and refinement

The synchrotron X-ray diffraction data were collected at the synchrotron facility (beamline B2, HASYLAB/DESY) in Hamburg from 12K to 773K (well above the paraelectric cubic phase transition) in steps of 10K. Low temperature (12K-300K) measurements were performed in a closed cycle capillary cryostat (Cryophysics) (Ihringer & Küster, 1993) while the high temperature measurements were performed using a capillary furnace from Stoe & Cie type 0.65.3. Data were recorded by a position sensitive image plate detector (OBI, *ortsfest auslesbarer Bildplattendetektor*) (Knapp, Joco *et al.*, 2004) at wavelengths between 0.6880Å - 0.6888 Å. More details about the experimental setup at the beamline can be found in the literature (Knapp, Baehtz *et al.*, 2004; Knapp, Joco *et al.*, 2004).

All the collected data were refined by the Rietveld method using the software package FULLPROF (Rodriguez- Carvajal, 2000). In *Amm2*, the different values of b_o and c_o lead to a rhombic distortion of the $(001)_c$ plane resulting in an expansion along $[110]_c$. The subscripts '*c*', '*o*', '*t*', and '*h*' denote the pseudocubic, orthorhombic, tetragonal, and rhombohedral unit cells respectively. Due to symmetry restrictions, the amount of refinable parameters in *Amm2*

is smaller than in *Pmm*2 and so *Amm*2 was used instead of *Pmm*2. *Amm*2 is set up in a way so that the polarisation vector is aligned along $[110]_c$.

The background under the peaks was refined using a linear interpolation between points from the regions in which no reflections contributed to the intensity. The model used was based on a T-C-H pseudo-Voigt profile function which is convoluted with asymmetry due to axial divergence as formulated by Laar et al (Laar & Yelon, 1984) and using the method of Finger et al (Finger *et al.*, 1994; Finger, 1998). The atomic positions and the isotropic atomic displacement parameters B_{iso} were refined. Efforts to refine the structure using anisotropic displacement parameters were not successful. The anisotropic peak broadening model in the general strain formulation from Stephens was used to refine the strain in the sample (Stephens, 1999).

2.3 Temperature-dependent measurement of electric properties

In order to compare the phase transition temperatures observed from the X-ray measurements with dielectric properties, dielectric measurements were carried out at elevated temperatures. The surfaces of the pellets were coated with silver paints which acted as electrodes for the dielectric measurement. The temperature dependence of the dielectric properties of the ceramics was measured with an LCR meter (HP 4284A, Agilent Technologies, Inc., Palo Alto, USA) connected to a heating chamber. The measurements were made from room temperature up to temperatures above the ferroelectric-paraelectric transitions for the respective samples using 5 °C temperature steps. The dielectric properties plots were made with data obtained at a frequency of 100 kHz.

Polarization and strain hysteresis measurements were carried out at room temperature using the standard Sawyer-Tower circuit and a complete dipolar hysteresis measurement was performed in 200 sec. Unipolar strain hysteresis measurement was used to determine the piezoelectric charge coefficient values.

3.0 Results and discussion

3.1 Structural characterization

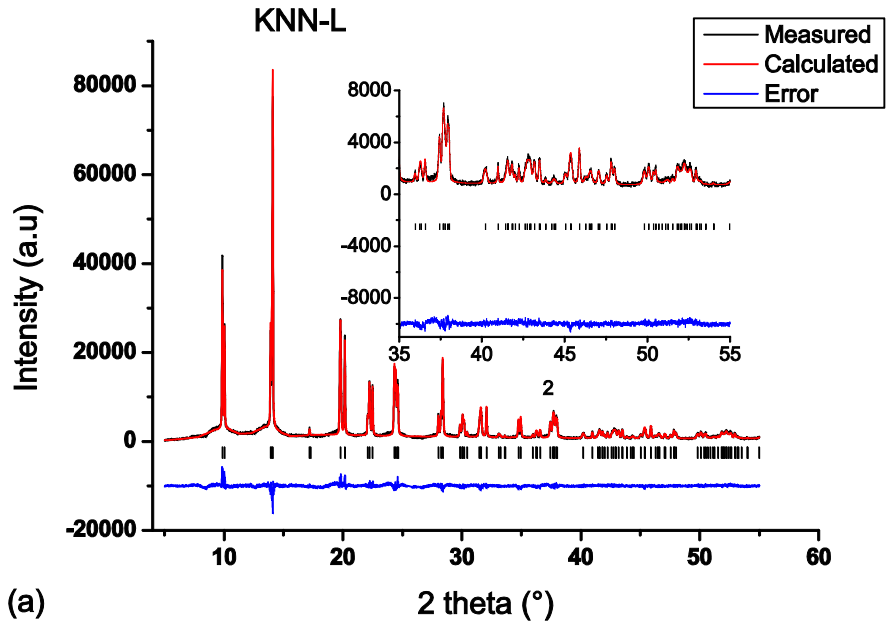

(a)

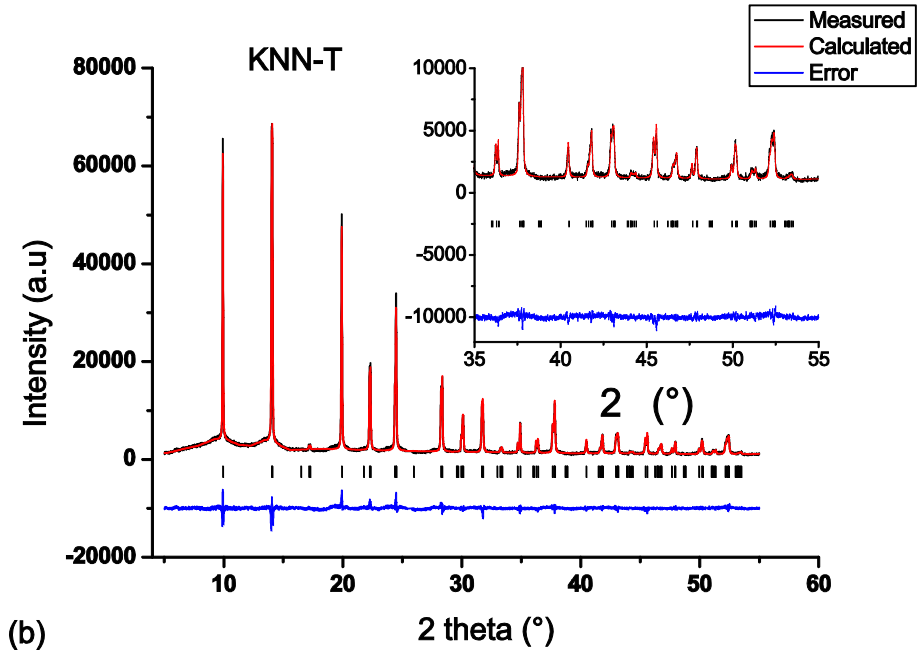

(b)

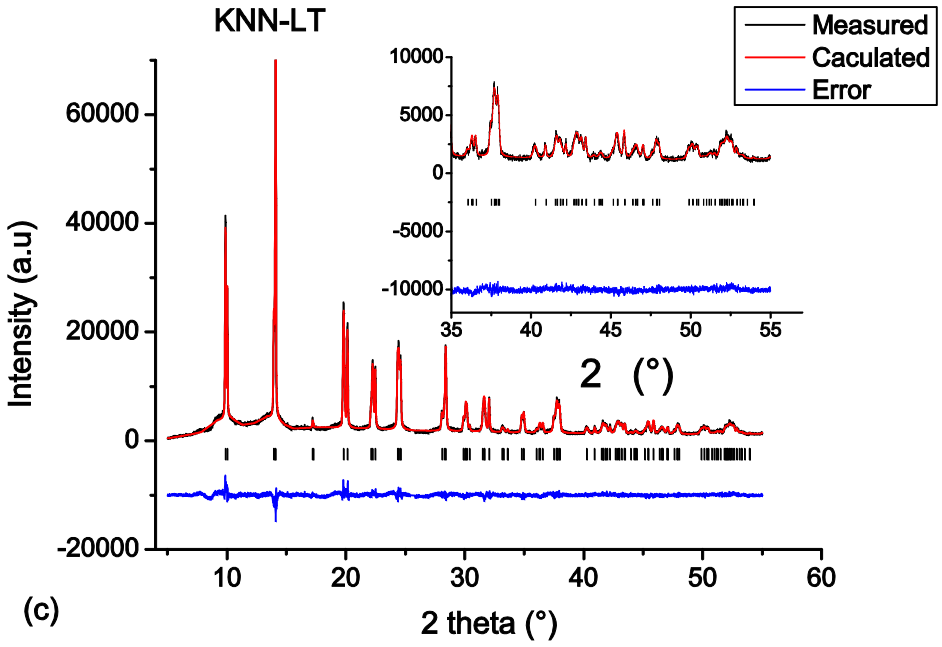

Figure 1 Measured and calculated synchrotron X-ray diffraction profiles and their difference curves for (a) KNN-L measured at 20K showing the orthorhombic phase, (b) KNN-T measured at 20K showing the rhombohedral phase and (c) KNN-LT measured at 20K showing the orthorhombic phase

The measured and calculated diffraction profiles and their difference curves for KNN-L, KNN-T and KNN-LT ceramics taken at 20K are shown in Fig. 1. KNN-L and KNN-LT (Figs. 1a and 1c) show an orthorhombic *Amm2* phase while KNN-T (Fig 1b) shows a rhombohedral *R3c* phase. The insets in the figures are enlarged sections of the patterns with higher 2-theta regions (35°- 55°). The clear splitting of the 200_c reflection at approx. 20° (Figs 1a and 1c) shows that the phase present is orthorhombic while for the rhombohedral phase (Fig 1b) the 200_c reflection shows no splitting. This indicates that the presence of Li^+ in KNN ceramics stabilizes the orthorhombic phase at lower temperatures by suppressing the orthorhombic to rhombohedral phase transition.

The refinement parameters for KNN-L, KNN-T and KNN-LT ceramics for the lowest temperatures of each model used for the refinement are shown in Tables 2, 3 and 4 respectively. The lattice parameters for KNN-L, KNN-T and KNN-LT ceramics as a function of temperature are shown in Fig. 2. Depending on the composition, a series of phase transformations were observed from 12K to temperatures above the respective T_c of the samples. Orthorhombic, rhombohedral, tetragonal and cubic phases were observed and for these phases, the space groups *Amm2*, *R3c*, *P4mm* and $Pm\bar{3}m$ were used for the refinement. There are temperature ranges where phase coexistence occurred and for such phase mixtures, a combination of the respective models was used for the refinement.

Table 2 Experimental details and refinement result for KNN-L at 12K, 373K, 393K and 753K

Phase type	Single	Two-phase		Single	Single
Crystal system	Orthorhombic	Orthorhombic	Tetragonal	Tetragonal	Cubic
space group	*Amm2*	*Amm*2	*P*4*mm*	*P*4*mm*	$Pm\bar{3}m$
Temp	12K	373K	373K	393K	753K
a (Å)	3.93132(3)	3.94646(4)	3.95257(8)	3.95531(3)	3.97596(16)
b (Å)	5.63895(5)	5.64422(7)			
c (Å)	5.68307(5)	5.67812(7)	4.03856(15)	4.03898(4)	
V ($Å^3$)	125.9851(17)	126.478(3)	63.094(3)	63.1878(10)	62.8532(4)
ρ (g/cm^3)	4.451	4.436		4.438	4.424
Z	2	2	1	1	1
Refinement					
Rp (%)	7.19	10.1		12.5	11.7
Rwp (%)	9.25	12.7		16.8	14.7
Rexp (%)	2.04	2.28		2.31	2.36
G O F	4.5	5.5		7.1	6.2
X^2	20.6	30.8		53.2	38.9
No of parameters	35	43	43	30	24

Table 3 Experimental details and refinement result for KNN-T at 12K, 170K, 190K, 443K and 643K.

Phase type	Single	Two-phase		Single	Single	Single
Crystal system	Rhombohedral	Rhombohedral	Othorhombic	Orthorhombic	Tetragonal	Cubic
space group	*R3c*	*R3c*	*Amm*2	*Amm*2	*P*4*mm*	$Pm\bar{3}m$
Temp	12K	170K	170K	190K	443K	643K
a (Å)	5.61271(4)	5.61662(5)	3.94036(6)	3.94128(2)	3.96331(2)	3.98276(19)
b (Å)			5.63778(12)	5.63739(4)		
c (Å)	13.83390(4)	13.83255	5.67068(10)	5.67081(4)	4.02016(3)	
V ($Å^3$)	377.417(4)	377.905(5)	125.974(4)	125.9970(14)	63.1479(6)	63.1758(5)
ρ (g/cm^3)	4.726	4.720		4.719	4.709	4.704
Z	6	6	2	2	1	1
Refinement						
Rp (%)	6.38	6.50		6.34	8.33	9.22
Rwp (%)	8.38	8.56		8.23	10.6	12.1
Rexp (%)	1.91	3.76		1.89	2.14	2.20
G O F	4.4	4.5		4.4	7.1	5.5
X^2	19.2	20.66		19.0	24.6	30.2
No of parameters	27	35		35	30	20

Table 4 Experimental details and refinement result for KNN-LT at 12K, 293K, 383K and 693K.

Phase type	Single	Two-phase		Single	Single
Crystal system	Orthorhombic	Orthorhombic	Tetragonal	Tetragonal	Cubic
space group	Amm2	*Amm*2	*P*4*mm*	*P*4*mm*	$Pm\bar{3}m$
Temp	12 K	293K	293K	383K	693K
a (Å)	3.93602(3)	3.94594(5)	3.95505(12)	3.95496(2)	3.96519(2)
b (Å)	5.63331(6)	5.6418(2)			
c (Å)	5.67188(6)	5.66929(11)	4.0038(5)	4.02479(3)	4.01483(3)
V ($Å^3$)	125.761(2)	126.212(5)	62.629(8)	62.9544(7)	63.1240(7)
ρ (g/cm^3)	4.709	4.701		4.703	4.693
Z	2	2	1	1	1
Refinement					
Rp (%)	6.26	4.50		6.08	6.17
Rwp (%)	8.06	5.70		8.05	7.85
Rexp (%)	1.81	1.51		1.21	1.75
G O F	4.4	3.8		6.6	4.5
X^2	19.7	14.3		44.1	20.2
No of parameters	35	46		30	30

The orthorhombic cell parameters b_o and c_o for all the graphs in Fig. 2 were divided by √2 while the rhombohedral cell parameters a_h and c_h were divided by √2 and √12 respectively for better representation so that they will fit well with a_t and c_t from the tetragonal phase.

KNN-L (Fig. 2a) exhibits an orthorhombic phase from 12K to 363K. Between 373K and 383K, phase coexistence between the orthorhombic and the tetragonal phase could be observed. The tetragonal phase existed from 393K to 743K and above this temperature the cubic phase was present. In KNN-T (Fig. 2b) the rhombohedral phase was observed from 12K to 160K with a two-phase coexistence of the rhombohedral and orthorhombic phase between 170K and 180K. From 190K to 423K the orthorhombic phase was present showing a two-phase coexistence of the orthorhombic and the tetragonal phase at 433K. From 453K to 633K the tetragonal phase was observed and above 643K the sample was cubic. In KNN-LT (Fig. 2c) the orthorhombic phase was present from 12K to 240K with a broad, two-phase coexistence of the orthorhombic and the tetragonal phase between 250K and 373K. The tetragonal phase was present from 383K to 693K and above this temperature, the cubic phase was present.

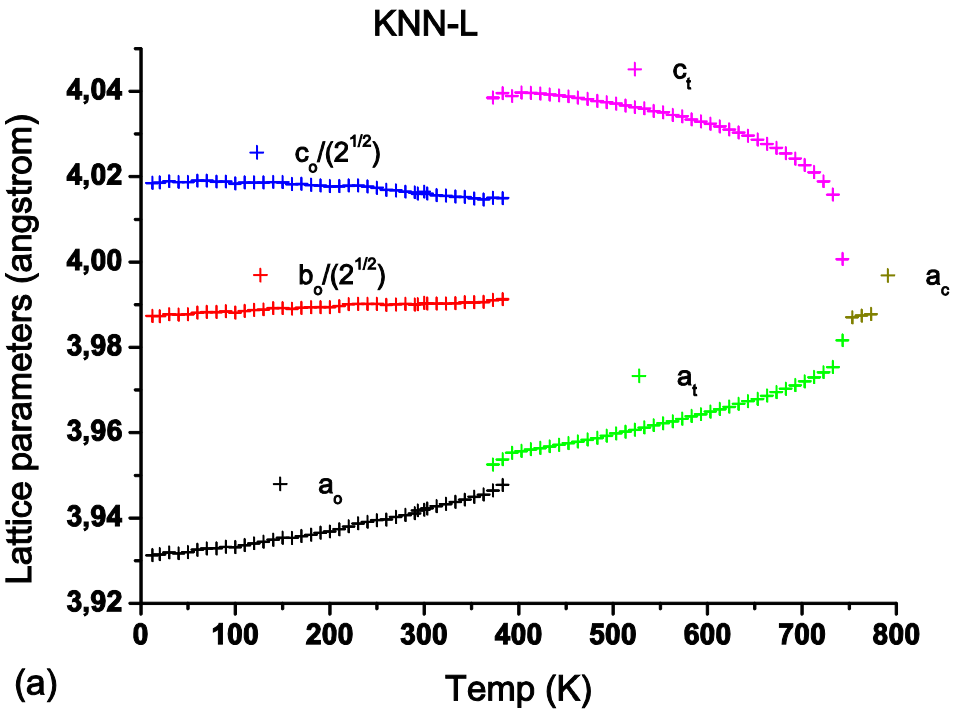
KNN-L
Lattice parameters (angstrom)
4,04
4,02
4,00
3,98
3,96
3,94
3,92
0
100
200
300
400
500
600
700
800
Temp (K)
c_t
c_o/(2^1/2)
b_o/(2^1/2)
a_c
a_t
a_o

(a)

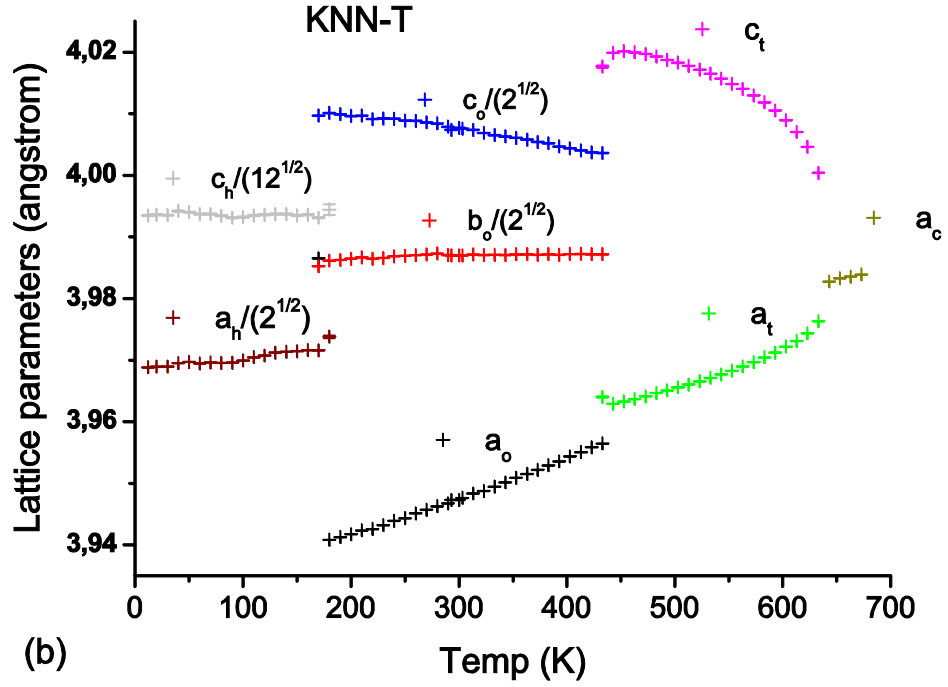
KNN-T
Lattice parameters (angstrom)
4,02
4,00
3,98
3,96
3,94
0
100
200
300
400
500
600
700
Temp (K)
c_t
c_o/(2^1/2)
c_h/(12^1/2)
b_o/(2^1/2)
a_c
a_h/(2^1/2)
a_t
a_o

(b)

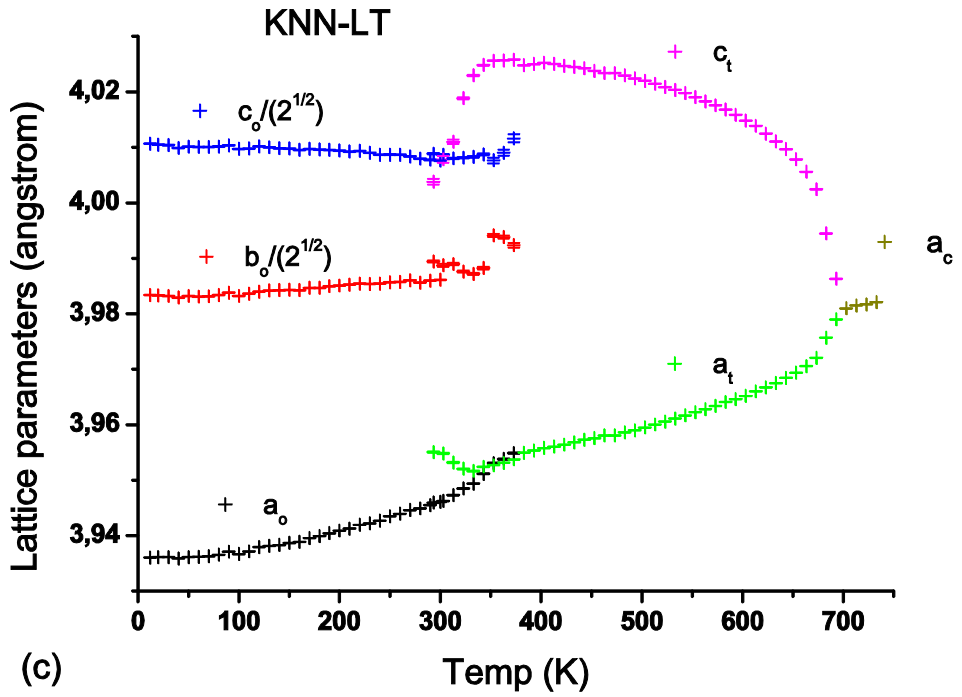

Figure 2 Temperature dependence of the lattice parameters (Å) a_h, c_h for the rhombohedral phase, a_o, b_o, c_o for the orthorhombic phase, a_t, c_t for the tetragonal phase and a_c for the cubic phase for (a) KNN-L ceramics with coexistence of the orthorhombic and tetragonal phase between 373K and 383K (b) KNN-T ceramics with phase coexistence between the rhombohedral and orthorhombic phase between 170K and 180K and orthorhombic and tetragonal phases at 433K (c) KNN-LT ceramics with coexistence of the orthorhombic and tetragonal phases from 273K and 373K

Different values of b_o and c_o in *Amm2* space group lead to a rhombic distortion of the $(001)_c$ plane that results in an expansion along $[110]_c$. The pseudo-cubic lattice parameter a_{pc} was calculated using equation 1.

$$a_{pc} = \frac{\sqrt{b_o^2 + c_o^2}}{2} \qquad (1)$$

The pseudo-monoclinic angle β was derived from equation 2

$$\beta = 2\arcsin\left(\frac{c_o}{2a_{pc}}\right) \qquad (2)$$

The plot of the pseudo monoclinic angle as a function of temperature for KNN-L, KNN-T and KNN-LT is shown in Fig. 3. In all cases, the pseudo-monoclinic angle decreases with increasing temperature. The pseudo-monoclinic angle increased in the following order; KNN-T, KNN-LT and KNN-L which shows that such lattice deformation do not require monoclinic

symmetry. The scattering of the values obtained for the KNN-LT composition from ~280K corresponds to the two-phase coexistence between the orthorhombic and the tetragonal phase.

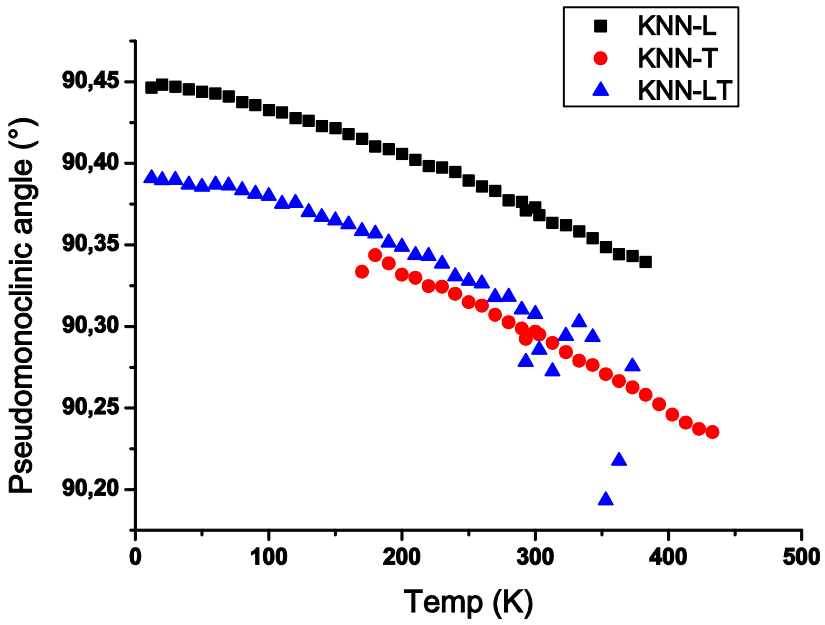

Figure 3 Pseudo-monoclinic angle as a function of temperature for KNN-L, KNN-T and KNN-LT ceramics.

The percentage of the constituent phases in the samples was calculated through the scale factors which involve the product of mass and volume of the unit cell contents of each phase. The weight fraction of the phase (W_P) was obtained using equation 3.

$$W_p = \frac{S_p(Z,M,V)_p * \tau_j}{\sum_j S_j(Z,M,V)_j * \tau_p} \qquad (3)$$

where W_P is the relative weight fraction of phase P in a mixture of j phases while S, Z, M, τ and V are the Rietveld scale factors obtained from the refinement, number of formula units per unit cell, mass of the formula unit, Brindley particle absorption contrast factor and unit cell volume respectively.

The weight fractions of the phases present in the samples as a function of temperature are shown in Fig. 4. In KNN-L (Fig 4a) the rhombohedral phase was not observed at low temperatures and the phase coexistence between the orthorhombic and the tetragonal phase occurred within a narrow temperature range between 373K and 383K. The temperature range of phase coexistence in KNN-LT was wider compared to the other compositions. The coexistence ranges from 240K to 383K. The temperature range of phase coexistence is even

wider (up to 453K) when Sb^{5+} is added to the sample (Mgbemere *et al.*, 2011). In KNN-T (Fig 4c) two different phase coexistence regions are observed. The first is between the rhombohedral and orthorhombic phase while the second is between the orthorhombic and the tetragonal phase. They occurred at between 170K and 180K for the former and at 433K for the later. The rhombohedral phase was observed in the KNN-T composition from 12K to 180K and to calculate the rhombohedral angle α_{pc} in the pseudocubic cell, the lattice parameters (a_h and c_h) of the hexagonal cell are used as shown in equation 4.

$$\cos\alpha_{pc} = \frac{\left(c_h^2 - 6a_h^2\right)}{\left(c_h^2 + 12a_h^2\right)} \tag{4}$$

The lattice strain is the deviation of the rhombohedral angle from 90° (Thomas, 1996; Zhang *et al.*, 2009) and the corresponding plot for KNN-T ceramics is shown in Fig. 5. As the temperature increased, the lattice strain gradually decreased and remained constant at the phase boundary.

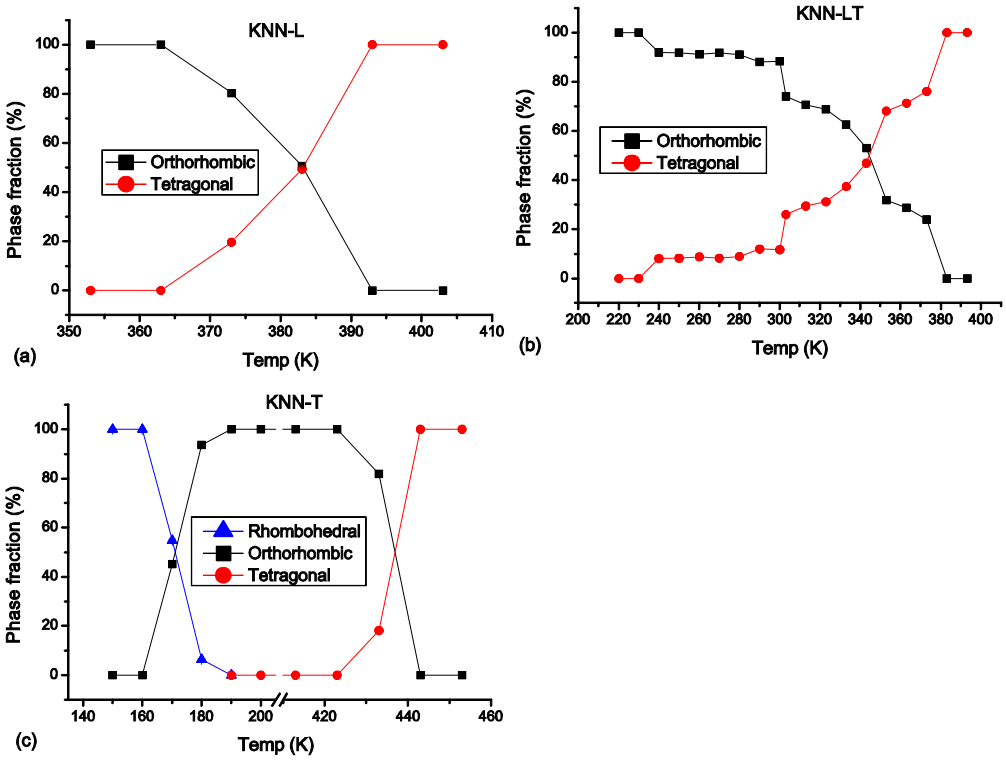

Figure 4 Weight fractions of the phases in percent as a function of temperature for (a) KNN-L, (b) KNN-LT and (c) KNN-T ceramics.

Domain formation and mechanical treatments on the ceramics during the synthesis and sample preparation steps are expected to introduce stresses and strain in the samples. Although the samples were annealed prior to being measured, all the stresses and strains may not be relieved and they contribute to lattice distortion. The distortions of the lattice (%) for

the rhombohedral, orthorhombic and tetragonal phases were calculated using equations 5, 6 and 7 respectively.

$$\eta(r) = \left(\left(\frac{c_h}{(\sqrt{6} * a_h)} \right) - 1 \right) * 100 \quad (5)$$

$$\eta(o) = \left(\left(\frac{c_o}{\sqrt{2} * a_o} \right) - 1 \right) * 100 \quad (6)$$

$$\eta(t) = \left(\left(\frac{c_t}{a_t} \right) - 1 \right) * 100 \quad (7)$$

The lattice distortion (%) as a function of temperature for the samples is shown in Fig. 6. The largest lattice distortions in both the orthorhombic and tetragonal phase were obtained from the KNN-L composition. In the orthorhombic phase, the distortion is ~ 2.25% and as the temperature increases, the distortion decreases. When a new phase is formed, the distortion jumps to a higher value and gradually decreases with increasing temperature. When the temperature approaches T_c, the distortion rapidly drops to near zero. The same trend was observed for the KNN-LT composition with the difference that the distortions are lower. The scattering of the distortion values corresponds to the two-phase coexistence in the sample. For KNN-T composition the degree of distortion in the rhombohedral phase is the smallest.

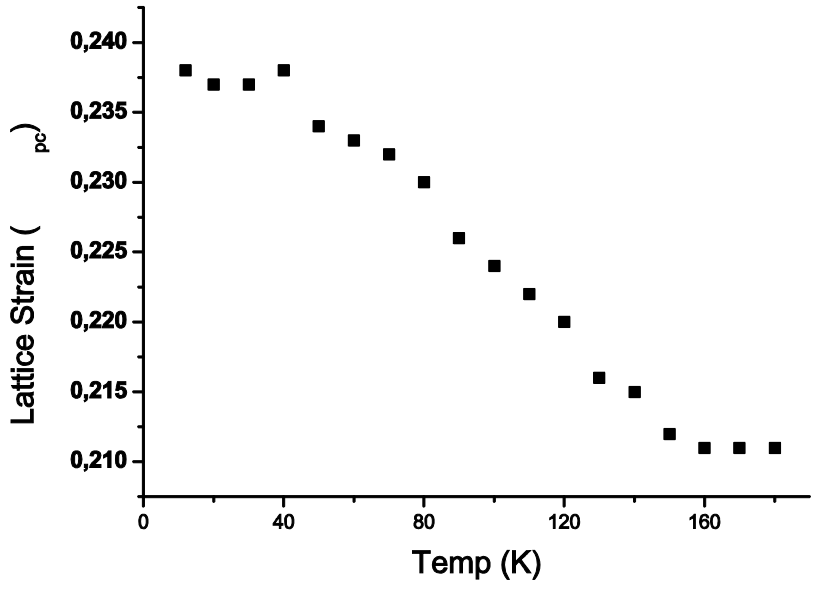

Figure 5 Lattice strain for KNN-T ceramics

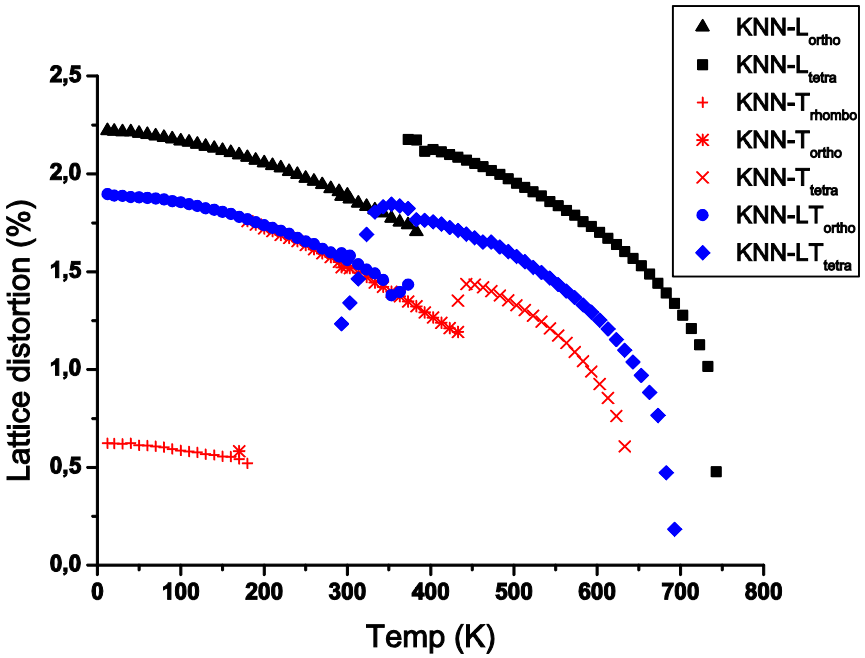

Figure 6 Lattice distortion (%) as a function of temperature (12K to 773K) for KNN-L, KNN-T and KNN-LT ceramics. Depending on the composition, rhombohedral, orthorhombic and tetragonal distortions were observed.

3.2 Electrical characterization

Plots of the dielectric properties for KNN-L, KNN-T and KNN-LT ceramics from room temperature to temperatures above their T_c are shown in Fig. 7.

The enlarged insets highlight the shape of the behavior near the tetragonal to orthorhombic phase transition ($T_{T\text{-}O}$). The temperatures at which the phase transitions occurred in the samples are slightly higher than those from the X-ray diffraction. A possible reason could be due to differences in strain constraints in the samples used for the measurements. The samples for X-ray diffraction were ground and annealed prior to the measurements while the samples used for dielectric measurements were in pellet form. The powders for X-ray diffraction were rotated during measurement to ensure that averaged results were obtained while fixed bulk ceramic pellets were used for the dielectric measurement. In a related article by Pramanick et al, (Pramanick *et al.*, 2011) polycrystalline constraints, domain wall motion and interphase boundary motion were said to have significant effects on the properties of the ceramics.

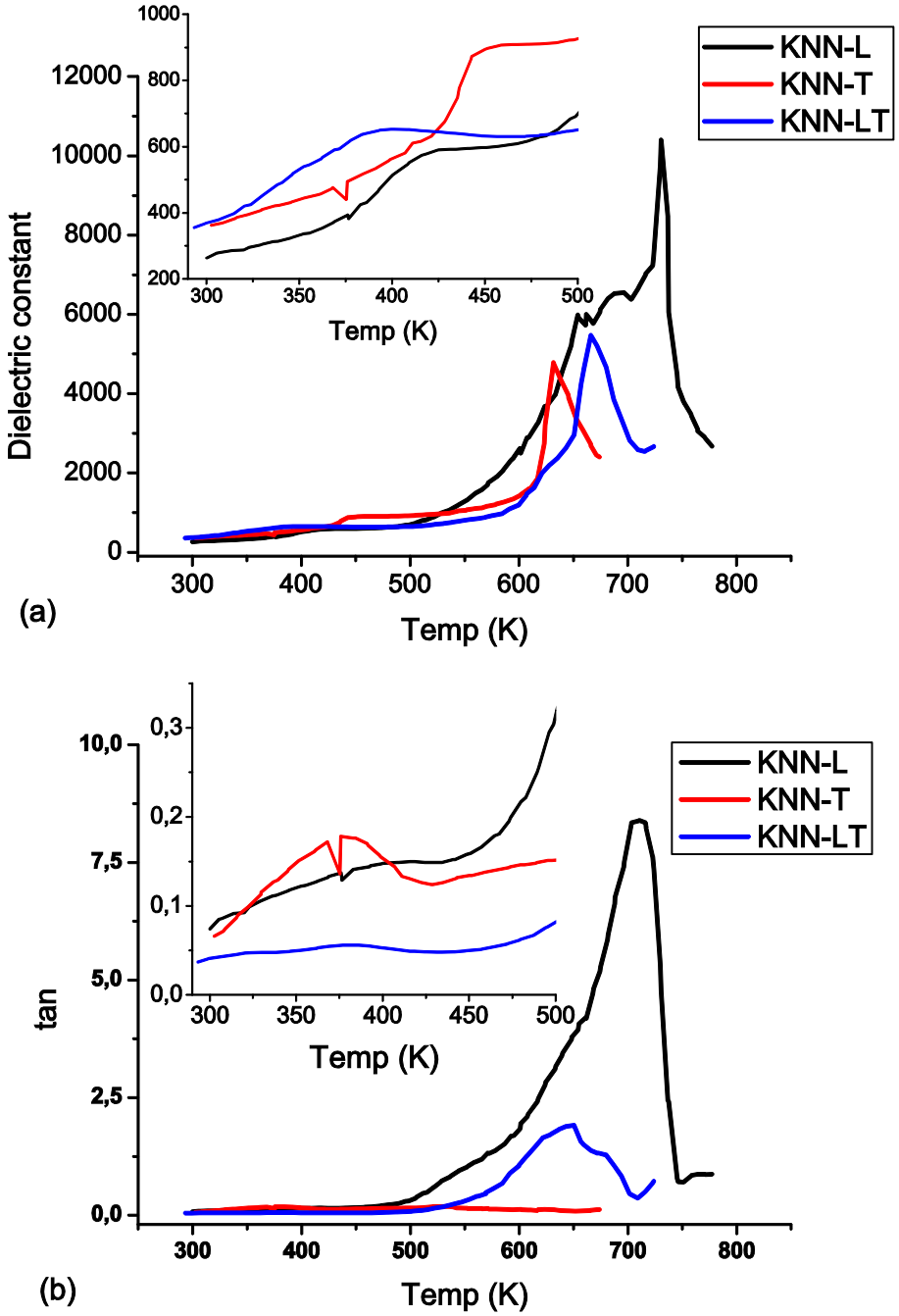

Figure 7 Variation of the (a) dielectric constant and (b) dielectric loss (tan δ) as a function of temperature for KNN-L, KNN-T and KNN-LT ceramics measured at 100 kHz.

For the KNN-L composition, the T_c with a peak value of ~10000 occurred at ~753K in the dielectric measurement and at ~730K with X-ray diffraction. In the KNN-T composition, the dielectric peak has a value of ~5000 and the corresponding T_c was observed at 631K whereas ~643K were detected with X-ray diffraction while for the KNN-LT composition, it was observed at ~666K (~5000) in the dielectric measurement and ~693K by X-ray diffraction. The variations in the reported T_c and $T_{T\text{-}O}$ values for similar compositions in the literature are

shown in Table 5. For the KNN-L composition, a T_{T-O} between ~393K-423K and T_c in the range 713K-733K with lower dielectric peak were reported (Du *et al.*, 2007; Klein *et al.*, 2007; Hollenstein *et al.*, 2005). For KNN-T-like compositions, reported T_{T-O} and T_c values were at ~460K and 623K-633K respectively (Matsubara *et al.*, 2005; Lin *et al.*, 2008) while for KNN-LT-like compositions, reported T_{T-O} and T_c values were approx. 293K and 623K-713K (Chang *et al.*, 2009; Zhao *et al.*, 2008). The shape of the peak at the T_{T-O} appears to be more diffuse with increasing temperature range of the phase coexistence in the material.

Table 5 Comparison of the reported phase transition temperatures obtained in this work with those reported in the literature for similar compositions

Composition	Ref.	T_c (K) X-ray	T_c (K) dielectric	T_{T-O} (K) dielectric
$(K_{0.47}Na_{0.51}Li_{0.03})(Nb_{0.97})O_{3.01}$ -KNN-L	This work	~753	~730	~416
$0.97(K_{0.5}Na_{0.5})NbO_3$–$0.03LiNbO_3$	(Klein *et al.*, 2007)		~700	~420
$0.96(Na_{0.5}K_{0.5})NbO_3$–$0.04LiNbO_3$	(Guo *et al.*, 2004)		~728	~398
$0.95(Na_{0.5}K_{0.5})NbO_3$–$0.05LiNbO_3$	(Du *et al.*, 2007)	~773	~753	~298
$(K_{0.49}Na_{0.51})$ $(Nb_{0.88}Ta_{0.1})O_3$ -KNN-T	This work	~643	~631.7	~450
$(KNa)_{0.97}(Nb_{0.9}Ta_{0.1})O_3$	(Matsubara *et al.*, 2005)		~633	~443
$(Na_{0.5}K_{0.5})(Nb_{0.9}Ta_{0.1})O_3$	(Lin *et al.*, 2008)		~633	~453
$(K_{0.47}Na_{0.51}Li_{0.025})$ $(Nb_{0.88}Ta_{0.1})O_{3.02}$ -KNN-LT	This work	~693	~666	
$(Na_{0.535}K_{0.48})_{0.942}$-$Li_{0.058}(Nb_{0.9}Ta_{0.1})O_3$	(Zhao *et al.*, 2008)		~703	~323
$(KNb)_{0.975}Li_{0.025}(Nb_{0.9}Ta_{0.1})O_3$	(Saito & Takao, 2006)		~648	
$(K_{0.46}Na_{0.5}Li_{0.04})(Nb_{0.85}Ta_{0.15})O_3$	(Chang *et al.*, 2009)		~643	~293

For KNN-T with very limited phase coexistence, the T_{T-O} (443K) appears to have a sharp kink. As the degree of phase coexistence increases, the shape of the curve becomes diffuse and the exact transition temperature cannot be clearly determined especially for KNN-LT composition (Fig. 7a). The dielectric loss in the samples is shown in Fig. 7b. In the KNN-L and KNN-T compositions high loss values were obtained compared to KNN-LT composition. As the measurement temperature increases, the loss values for KNN-L and KNN-T also increases but the loss values for KNN-LT remains approximately the same. This shows that the properties of KNN-LT can be stable over a wide temperature range.

The polarization hysteresis curves for the samples are shown in Fig. 8a. When a field of ~20 kV/cm is applied, hysteresis loops with near saturation polarization were obtained for some samples. A remnant polarization P_r value of 25 μC/cm^2 was obtained for KNN-L composition while the coercive field E_C was ~ 8 kV/cm for all compositions. For the KNN-T composition, the P_r was ~16.5 μC/cm^2 and was ~13 μC/cm^2 for the KNN-LT composition. P_r values in the literature (17-19μC/cm^2) for compositions close to KNN-T are similar but the only difference is that we used lower applied fields (Matsubara *et al.*, 2005). For KNN-LT

compositions, slightly higher P_r values (25 μC/cm^2) were reported in the literature (Chang *et al.*, 2009).

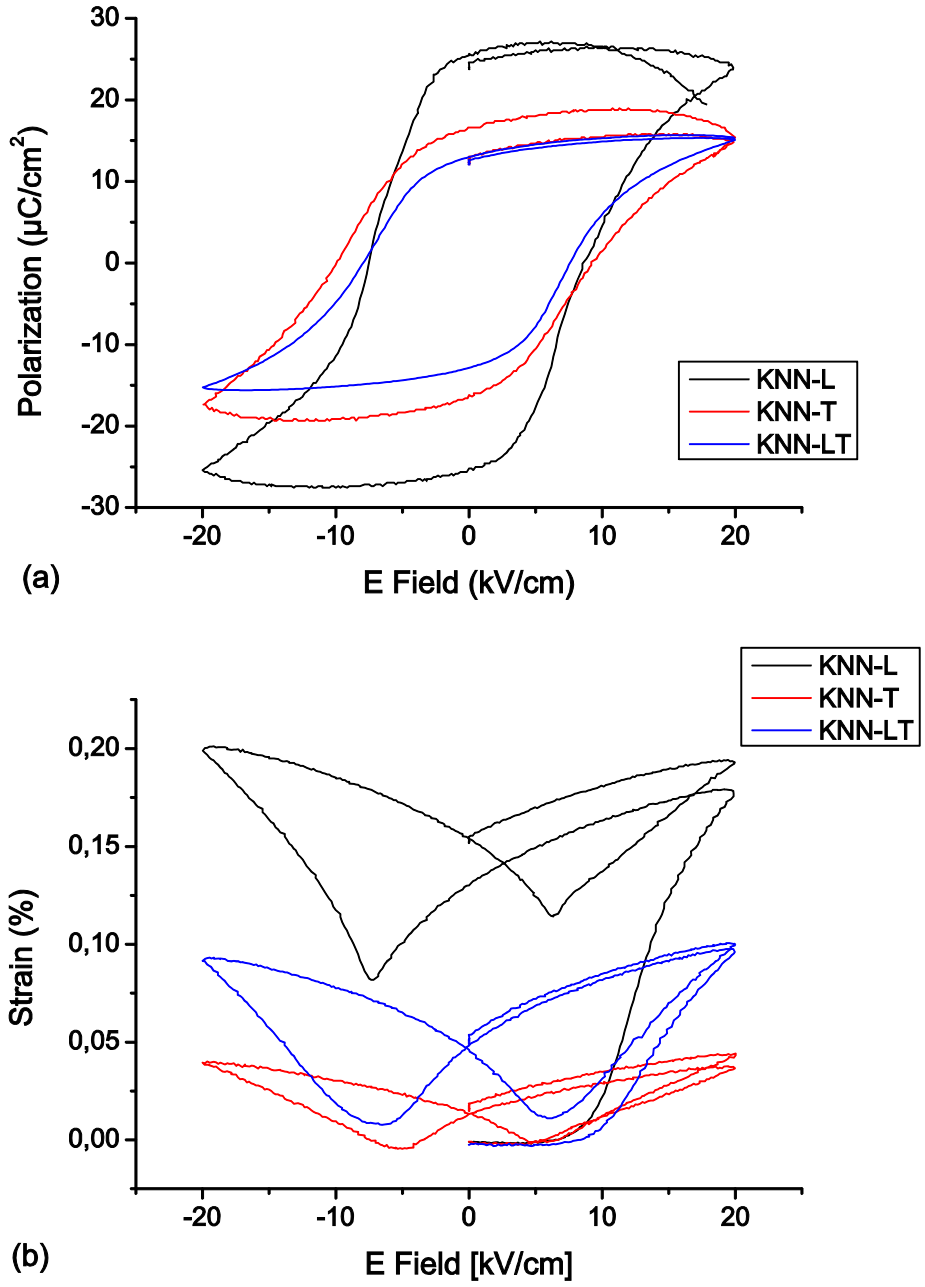

Figure 8 Variation of (a) polarization-field hysteresis loops and (b) strain-field hysteresis loops measured at room temperature for KNN-L, KNN-T and KNN-LT ceramics.

Table 6 Density, P_r, E_C and S_r values for KNN-L, KNN-T and KNN-LT ceramics studied at room temperature

Composition	Density (g/cm^3)	Theoretical density @ 293K (g/cm^3)	Remnant polarization P_r ($\mu C/cm^2$)	Coercive field E_C (kV/cm)	Remnant strain S_r	Piezoelectric coefficient d^*_{33} (pm/V)
KNN-L	4.12±0.04	4.44	25.0	8.0	0.0013	206.7±8.03
KNN-T	4.40±0.07	4.71	16.5	7.8	0.000136	103.5±15.13
KNN-LT	4.23±0.03	4.70	13.0	7.8	0.00047	227.99±6.45

The strain hysteresis loops for the samples showing the typical butterfly shape which indicates ferroelectricity are shown in Fig. 8b. High remnant strain S_r, (0.0013) was obtained for KNN-L composition which corresponds to the high lattice distortion for the sample in Fig. 6. Moderately high S_r was obtained for KNN-LT (0.00047) while a very low S_r (0.000136) was obtained for KNN-T composition. There are not much strain hysteresis data in the literature for these compositions with S_r values for comparison. The asymmetry in the loop for KNN-L composition is possibly due to uneven distribution of charges as the field is applied in opposite directions (Robels *et al.*, 1995; Lupascu & Rabe, 2002). The piezoelectric charge coefficient d^*_{33} values for the samples obtained using unipolar strain hysteresis measurements is shown in Table 6. The highest value (228±6 pm/V) is obtained with the KNN-LT composition followed by KNN-L with a value of 206±8 pm/V. The highest relative density value of ~93% was obtained with the KNN-T composition but the d^*_{33} was the lowest (103±15 pm/V). A slightly higher d_{33} value was reported for KNN-T composition and this increment was attributed to "softening" of the ceramic due to the presence of $KTaO_3$ (Lin *et al.*, 2008). For KNN-L compositions a slightly lower value was reported (Du *et al.*, 2007; Guo *et al.*, 2004) and for KNN-LT-like compositions, a range of values were reported depending on the composition (Chang *et al.*, 2009; Hollenstein *et al.*, 2005; Zhao *et al.*, 2008). A summary of the density, P_r, E_C, S_r and d^*_{33} values are shown in Table 6

3.3 Discussion

Materials which undergo a first order phase transition exhibit a discontinuity in the polarization, lattice parameters and other properties (Boettger, 2004). The lattice parameters for all the samples show discontinuities at the phase transitions (Fig. 2) indicating that they all undergo a first order phase transition. Noheda et al (Noheda *et al.*, 2002) reported that when there is a second order phase transition, no phase coexistence should be observed thereby confirming first order phase transition. It is not clear if the phase coexistence is an intrinsic feature of modified KNN ceramics or just a compositional fluctuation over a small range of temperature or composition. More research needs to be made to verify that.

The chemical composition and radii of the ions influence how ferroelectric phases are formed. Li^+ has a very small ionic radius (76 pm) compared to either K^+ (138 pm) or Na^+ (102 pm). Ta^{5+} being a transition element, has a lot of valence states with different ionic radii. If the valence state is +5, the ionic radius is similar to Nb^{5+} (64 pm) but as the valence state decreases, the ionic radius increases (Shannon, 1976). The huge difference in the ionic radius of Li^+ compared to A-site elements which it replaces may explain why the rhombohedral low temperature phase is suppressed while T_c is shifted to higher temperatures. Similar results have been reported for Ca^{2+} and Pb^{2+} doped $BaTiO_3$ where the T_c increased with doping while other phase transition temperatures decreased (Mitsui & Westphal, 1961). Both elements have a smaller ionic radius compared to Ba^{2+} giving them more space and higher atomic and electronic polarizability respectively, which intensifies the interactions between the Ti^{4+} ions (Mitsui & Westphal, 1961).

Addition of dopants is known to result in the lowering of the phase transition temperatures (Zhang *et al.*, 2007). Instead of the normal morphotropic phase boundary that is observed in PZT, a polymorphic phase transition (PPT) occurs and this is both a composition and temperature dependent phenomenon. Phase coexistence leads to the formation of a polymorphic phase boundary which results in higher piezoelectric properties compared to pure KNN especially for isovalent dopants (Zhang *et al.*, 2007). The increase in the number of possible polarization directions is also a possible reason for the enhanced properties. A total of 18 possible polarization directions of the domains are therefore available for a mixture of orthorhombic (12 $[110]_c$) and tetragonal phases (6 $[001]_c$).

As the temperature range of the phase coexistence becomes wider, the piezoelectric coefficient becomes higher especially for KNN with Li, Ta and Sb (Saito *et al.*, 2004; Mgbemere *et al.*, 2009) but unlike in PZT, the enhancement in the d_{33} value is not extremely high at the phase boundary.

The dielectric constant values always peak at T_c because the polarizability of the lattice is higher and is also associated with the increased density of free conducting electrons (Damjanovic, 2005). The highest value of dielectric constant at T_c was obtained with the KNN-L composition (Fig.7a) and it also has the highest dielectric loss values. As the temperature increases, it is probable that there is motion of Li^+ in the lattice which creates interfacial ionic polarization within the Nb-O framework giving rise to large dielectric constants (Glass et al., 1977). This motion of the Li^+ also accounts for the high dielectric loss in KNN-L composition. It can also be explained in terms of the mobility of the free electronic or ionic charges in the sample leading to ease of domain wall movement and therefore high

dielectric loss. When Ta^{5+} is added to the Li^{+} (KNN-LT), it appears that this motion is reduced in the lattice leading to reduced dielectric constant and loss values.

A decrease in the lattice distortion also results in a reduction of both the spontaneous polarization and strain (Hoffmann *et al.*, 2004). The high P_r value for KNN-L is related to the high lattice distortion at all temperatures. Addition of Ta^{5+} to the Li^{+} (KNN-LT) decreases the lattice distortion, the spontaneous polarization and S_r. KNN-T composition has low distortion values possibly because Ta^{5+} inhibits the domain wall movement due to large concentration of defects (Saito & Takao, 2006). It reduces the average grain size in KNN which results in higher relative density values. The uneven strain hysteresis loop for KNN-L (Fig. 8b) is possibly due to inhomogeneities in the charge carrier densities in the sample (Robels *et al.*, 1995). The d^*_{33} value for the KNN-T composition is low even when the relative density is higher than other compositions possibly due to the difficulty of aligning the domains when the electric field is applied.

4.0 Conclusion

Synchrotron X-ray diffraction was used to characterize KNN ceramics modified with Li^{+} and Ta^{5+} from 12K to temperatures above their respective T_c using a 10K measurement step. OES/ICP analysis showed that after sintering, the presence of elements with high vapor pressure (Li^{+} and K^{+}) is lower than the intended compositions and that small amounts of ZrO_2 are introduced into the samples. Li^{+} in KNN suppresses the formation of the rhombohedral low temperature phase and this is attributed to the size difference between the ionic radii of the A-site elements. When only Ta^{5+} is added to KNN, the $T_{r\text{-}o}$ is observed at ~170K. With co-doping of Li^{+} and Ta^{5+} in KNN, a wide temperature range of phase coexistence is observed with a slightly higher piezoelectric coefficient due to higher number of possible polarization directions. High dielectric constant peaks, lattice distortion, spontaneous polarization and strain and dielectric constants are obtained with Li^{+} doped KNN ceramics. This is attributed to the ease of domain wall movement, and high mobility of the free electrons or ionic charges in the sample. A higher density value does not always translate to high piezoelectric properties as there are other determining factors involved.

Acknowledgements The research leading to these results has received financial support from Deutsche Forschungsgemeinschaft (DFG) under the grant No: SCHN 372/16-1 and Bundesministerium für Bildung und Forschung project grant No. 05K10ODA.

References

Boettger, U. (2004). *Polar oxides*, edited by R. Waser, U. Boettger & S. Tiedke, pp. 11-37. Weinheim: Wiley-VCH.

Chang, Y., Yang, Z., Ma, D., Liu, Z. & Wang, Z. (2009). *J. Appl. Phys.* **105**.

Damjanovic, D. (2005). *J. Am. Ceram. Soc.* **88**, 2663-2676.

Du, H., Zhou, W., Luo, F. & Zhu, D. (2007). *Appl. Phys. Lett* **91**.

Egerton, L. & Dillion, D. M. (1959). *J. Am. Ceram. Soc* **42**, 438-442.

Finger, L. W. (1998). *J. Appl. Cryst.* **31**, 111.

Finger, L. W., Cox, D. E. & Jephcoat, A. P. (1994). *J. Appl. Cryst.* **27**, 892-900.

Guo, Y., Kakimoto, K.-i. & Ohsato, H. (2004). *Appl. Phys. Lett.* **85**, 4121-4123.

Hagh, N. M., Jadidian, B., Ashbahian, E. & Safari, A. (2008). *IEEE-UFFC Transactions* **55**, 214-224.

Hippel, A. V. (1950). *Modern Physics* **22**, 221-237.

Hoffmann, M. J., Kungl, H., Reszat, J.-T. & Wagner, S. (2004). *Polar oxides*, edited by R. Waser, U. Boettger & S. Tiedke, Weinheim: Viley-VCH.

Hollenstein, E., Damjanovic, D. & Setter, N. (2007). *J. Eur. Ceram. Soc.* **27**, 4093-4097.

Hollenstein, E., Davis, M., Damjanovic, D. & Setter, N. (2005). *Appl. Phys. Lett* **87**.

Ichinose, N. & Udagawa, K. (1995). *Ferroelectrics* **169**, 317-325.

Ihringer, J. & Küster, A. (1993). *J Appl. Cryst.* **26**, 135-137.

Klein, N., Hollenstein, E., Damjanovic, D., Trodahl, H. J. & Setter, N. (2007). *J. Appl. Phys.* **102**.

Knapp, M., Baehtz, C., Ehrenberg, H. & Fuess, H. (2004). *J. Synchrotron Rad.* **11**, 328-334.

Knapp, M., Joco, V., Baehtz, C., Brecht, H. H., Berghaeuser, A., Ehrenberg, H., Seggern, H. v. & Fuess, H. (2004). *Nuclear Instruments and Methods in Phys. Research A* **521**, 565-570.

Laar, B. V. & Yelon, W. B. (1984). *J. Appl. Cryst.* **17**, 47-54.

Lee, S.-M., Lee, S.-H., Yoon, C.-B., Kim, H.-E. & Lee, K.-W. (2007). *J. Electroceram.* **18**, 311-315.

Lin, D., Kwok, K. W. & Chan, H. L. W. (2008). *Appl. Phys. A* **91**, 167-171.

Lufaso, M. W., Barnes, P. W. & Woodward, P. M. (2006). *Acta Cryst.* **B62**, 397-410.

Lupascu, D. C. & Rabe, U. (2002). *Phys. Rev. Lett.* **89**, 187601

Matsubara, M., Yamaguchi, T., Sakamoto, W., Kikuta, K., Yogo, T. & Shin-ichi, H. (2005). *J. Am. Ceram. Soc.* **88**, 1190–1196.

Mgbemere, H. E., Fernandes, R. P., Hinterstein, M. & Schneider, G. A. (2011). *Z. Kristallogr.* **226**, 138-144.

Mgbemere, H. E., Herber, R.-P. & Schneider, G. A. (2009). *J. Eur. Ceram. Soc.* **29**, 1729-1733.

Mgbemere, H. E., Schneider, G. A. & A.Stegk, T. (2010). *Funct. Mat. Lett.* **3**, 25-30.

Mitsui, T. & Westphal, W. B. (1961). *Phys. Rev.* **124**, 1354-1359.

Noheda, B., Cox, D. E., Shirane, G., Ye, Z.-G. & Gao, J. (2002). *Phys. Rev. B* **66**, 1-10.

Noheda, B., Gonzalo, J. A., Cross, L. E., Guo, R., Park, S. E., Cox, D. E. & Shirane, G. (2000). *Phys. Rev. B* **61**, 8687 - 8695.

Pramanick, A., Damjanovic, D., Daniels, J. E., Nino, J. C. & Jones, J. L. (2011). *J. Am. Ceram. Soc.* **94**, 293-309.

Robels, U., Calderwood, J. H. & Arlt, G. (1995). *J. Appl. Phys.* **77**, 4002-4008.

Rodriguez- Carvajal, J. (2000).

Saito, Y. & Takao, H. (2006). *Ferroelectrics* **338**, 17–32.

Saito, Y., Takao, H., Tani, T., Nonoyama, T., Takatori, K., Homma, T., Nagaya, T. & Nakamura, M. (2004). *Nature* **432**, 84-87.

Shannon, R. D. (1976). *Acta Cryst.* **A32**, 751-767.

Shirane, G., Newnham, R. & Pepinsky, R. (1954). *Phys. Rev.* **96**, 581-588.

Skidmore, T. A., Comyn, T. P. & Milne, S. J. (2009). *Appl. Phys. Lett.* **94**.

Stephens, P. W. (1999). *J Appl. Cryst.* **32**, 281-289.

Takenaka, T., Okuda, T. & Takegahara, K. (1997). *Ferroelectrics* **196**, 175-178.

Thomas, N. W. (1996). *Acta Cryst.* **B52**, 954-960.

Zhang, N., Glazer, A. M., Baker, D. & Thomas, P. A. (2009). *Acta Cryst.* **B65**, 291-299.

Zhang, S., Xia, R. & Shrout, T. R. (2007). *J. Electroceram.* **19**, 113-126.

Zhao, P., Zhang, B.-P. & Li, J.-F. (2007). *Appl. Phys. Lett* **90**.

Zhao, P., Zhang, B.-P. & Li, J.-F. (2008). *J. Am. Ceram. Soc.* **91**, 1690-1692.

Zuo, R., Fu, J., Su, S., Fang, X. & Cao, J.-L. (2009). *J. Mater Sci:Mater Electron* **20**, 212-216.